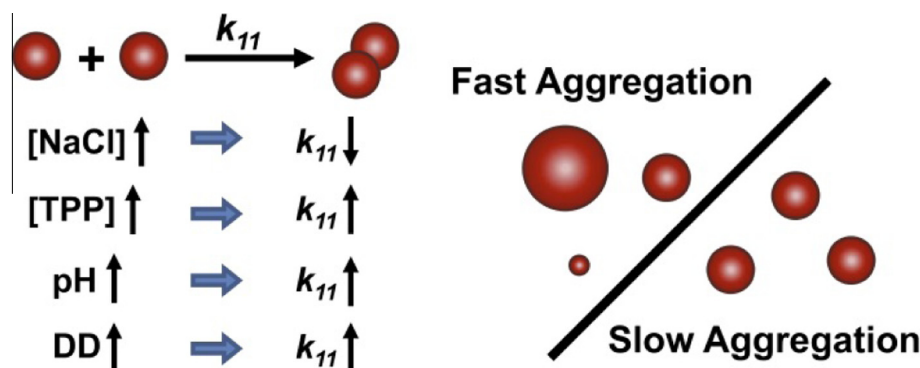


## Regular Article

## On the kinetics of chitosan/tripolyphosphate micro- and nanogel aggregation and their effects on particle polydispersity

Yan Huang<sup>a,1</sup>, Yakov Lapitsky<sup>a,b,\*</sup><sup>a</sup> Department of Chemical and Environmental Engineering, University of Toledo, Toledo, OH 43606, United States<sup>b</sup> School of Green Chemistry and Engineering, University of Toledo, Toledo, OH 43606, United States

## GRAPHICAL ABSTRACT



## ARTICLE INFO

## Article history:

Received 8 July 2016

Revised 21 September 2016

Accepted 22 September 2016

Available online 23 September 2016

## Keywords:

Chitosan

Tripolyphosphate

Microgels

Nanoparticles

Ionic crosslinking

Aggregation

Polydispersity

## ABSTRACT

Submicron chitosan/tripolyphosphate (TPP) particles are widely investigated as nanocarriers for drugs, genes and vaccines. One of the key particle properties that requires control is their size distribution, which depends on the extent of chitosan/TPP primary nanoparticle aggregation into higher-order submicron colloids. To provide a better understanding of this higher-order aggregation process, this study analyzes the factors that control chitosan/TPP particle aggregation kinetics in the presence of free TPP (such as present during particle formation). The aggregation rates exhibit a sharp power-law decrease with the monovalent salt concentration and a power-law increase with the free TPP concentration. Moreover, the aggregation rates increase with the pH and with the chitosan degree of deacetylation (DD). These variations in aggregation rates reflect the effects of monovalent salt, TPP concentration, pH and chitosan DD on particle bridging by the surface-bound TPP. Furthermore, these aggregation rates are much faster than those predicted based on Derjaguin and Landau, Verwey and Overbeek (DLVO) interaction potentials, which might reflect nonuniformities in particle shape and charge, and/or complications caused by particle softness. Finally, implications of the above aggregation kinetics on the uniformity of chitosan/TPP micro- and nanogel size are analyzed, where we: (1) show how particle polydispersity can be diminished by lowering the chitosan DD; and (2) explain the opposing results on how chitosan/TPP particle polydispersity is affected by monovalent salt.

© 2016 Elsevier Inc. All rights reserved.

\* Corresponding author at: Department of Chemical and Environmental Engineering, University of Toledo, Toledo, OH 43606, United States.

E-mail address: [yakov.lapitsky@utoledo.edu](mailto:yakov.lapitsky@utoledo.edu) (Y. Lapitsky).

<sup>1</sup> Current address: College of Biological Science and Engineering, Fuzhou University, Fuzhou, Fujian 350108, China.

## 1. Introduction

Submicron particles prepared through the ionic crosslinking of chitosan with tripolyphosphate (TPP) are widely investigated as

potential vehicles for drug and gene delivery [1–8]. They form under very mild, aqueous conditions (which help preserve the bioactivity of their payloads) [9], are mucoadhesive [10,11] and can facilitate drug transport across epithelial membranes [8,11]. Consequently, they attract special interest for ocular [4,12] and intranasal [8,13] administration of bioactive payloads ranging from small molecules [4,8,14], to protein drugs and vaccines [1,5,6], to polynucleotides [3,15].

To ensure their optimal performance, it is vital to control their size distributions. To this end, numerous experimental studies have been performed [2,14,16,17]. These revealed a variety of guidelines (sometimes conflicting ones) on tuning both the particle average size and polydispersity. The average particle size, for instance, has generally been shown to increase with the concentration of the parent chitosan solution and the chitosan molecular weight [14,17,18]. Likewise, chitosan/TPP particle size and colloidal stability were demonstrated to be sensitive to the TPP:chitosan ratio [14,16,17,19]. When the chitosan monomer (glucosamine) binding sites were in excess, the particle sizes typically decreased with the TPP:glucosamine molar ratio, due to an evident decrease in swelling [16,17,19]. Conversely, when multivalent TPP was present in excess, the particles aggregated and ultimately precipitated [14,16,19].

In addition to controlling their average size, significant attention has been devoted to minimizing chitosan/TPP particle polydispersity [14,16,18–21]. Approaches to doing this have included use of parent chitosan molecules with low molecular weights [14,18], preparation of chitosan samples with highly-uniform molecular weights and degrees of deacetylation (DD) [21], or varying process and formulation parameters such as the chitosan and TPP concentrations [14,18,19], preparation temperature [16] and pH [14,20], and mixing procedures [16,18]. Recently, we and others have shown that (provided that the ionic strength is not high enough to inhibit particle formation) preparation of chitosan/TPP particles in the presence of monovalent salt can drastically reduce particle polydispersity [19,22]. Conversely, Bugnicourt et al., who prepared chitosan/TPP particles with narrow size distributions without the use of salt (by using highly-deacetylated chitosan with a narrow molecular weight distribution [21]), have made opposite observations, where the polydispersities were generally higher at elevated ionic strengths [18]. Such conflicting results have also been reported in studies examining variations in average particle size. Despite studying similar TPP:chitosan ratios, for instance, some groups reported the particle size to increase with the TPP:chitosan ratio [14], others reported the average particle size to decrease with the TPP:chitosan ratio [17,23], and others yet reported non-monotonic TPP:chitosan ratio effects on particle size (where a maximum or minimum particle size occurred at intermediate ratios) [21,22,24]. Consequently, chitosan/TPP micro- and nanogel size is tuned through trial and error, with few reliable guidelines for achieving predictable control, and limited understanding of the underlying molecular and colloidal interactions.

Despite this limited understanding, the dependence of chitosan/TPP particle size on the method by which the chitosan and TPP are mixed [20,25] clearly indicates that particle size distributions are kinetically controlled. To gain further mechanistic insight into their formation kinetics, we have recently shown these particles to form through a two-step mechanism, where primary 20–50 nm nanoparticles form and then aggregate into the larger, higher-order colloids that are obtained at the end of particle formation process [26]. Thus, the ultimate size distributions of chitosan/TPP particles reflect the extent of their secondary/higher-order aggregation [26], whose understanding could enable better control over particle size.

The aggregation events that underlie the ultimate chitosan/TPP micro- and nanogel size require the particles to: (1) collide (i.e.,

establish surface-to-surface contact); and (2) stick together upon colliding [27]. For lyophobic colloids, it is assumed that the particles always stick (i.e., aggregate) upon colliding due to their strong van der Waals attraction, which dominates at short distances and holds the particles together once they overcome the longer-range electrostatic energy barrier [28]. Conversely, contact between lyophilic particles does not always lead to sticking, due to either a much weaker van der Waals attraction [27,29,30], or repulsive solvation [31] and/or steric forces [32]. This is exemplified in a study by Wu et al., where poly(*N*-isopropylacrylamide) (pNIPAm) microgels (in their water-swollen states) behaved thermodynamically as hard spheres and did not stick upon colliding [29,33]. This lyophilicity was attributed to the similarity in Hamaker constants between the suspending aqueous medium and water-swollen microgel phases (in other words, negligibly weak van der Waals forces) [29].

Recently, we have postulated that similar phenomena might occur in the case of chitosan/TPP particles [26,27], which are also water-rich [22,34] and have, at least qualitatively, been reported to become more (rather than less) colloiddally stable when monovalent salt is added – i.e., increasing their collision frequency does not increase their aggregation rate [19,35]. Even when the van der Waals attraction is weak, however, such lyophilic particles can still flocculate (or aggregate) through bridging and depletion mechanisms [28]. Bridging flocculation occurs when a flocculant (in this case TPP) simultaneously binds to two particles and causes aggregation by “bridging” the particles together. This bridging has been proposed as the dominant aggregation mechanism during the formation of chitosan/TPP micro- and nanogels [14,19]. Still lacking, however, is a quantitative and systematic analysis of the factors that control the kinetics of this aggregation. Indeed, despite the extensive literature on colloidal aggregation rates [36–38], data on the aggregation rate constants of even other types of polymeric micro- and nanogels (e.g., those formed through covalent crosslinking) remains very limited [39].

Here, to gain quantitative insight into how various parameters (i.e., NaCl concentration, TPP concentration, pH and DD-values) affect these aggregation rates, the size evolutions of aggregating chitosan/TPP particles are investigated by light scattering. Though chitosan/TPP particles are typically formed using TPP-limited conditions (so that their aggregation stops once the free TPP is depleted), this study investigates chitosan/TPP particle aggregation in an excess of TPP – i.e., by adding TPP to preformed particles with nearly saturated TPP binding sites. This keeps the free TPP concentration roughly constant throughout each aggregation experiment, so that aggregation rate constants can be obtained from the light scattering data. To further explore the aggregation mechanism, these aggregation rate constants are then compared with the particle collision rates predicted based on Fuchs theory and Derjaguin and Landau, Verwey and Overbeek (DLVO) interaction potentials [28,40,41]. Finally, the impacts of these aggregation rates on chitosan/TPP particle polydispersity are discussed, where we: (1) demonstrate how particle polydispersity can be lowered by reducing the chitosan DD; and (2) explain the conflicting results on how their polydispersity is affected by monovalent salt.

## 2. Materials and methods

### 2.1. Materials

Millipore Direct-Q 3 deionized water (18.2 M $\Omega$  cm) was used in all experiments. Chitosan (viscosity-average molecular weight,  $M_v$  = 80 kDa [42]), TPP and NaCl were purchased from Sigma-Aldrich (St. Louis, USA). The chitosan DD was determined to be 91% by pH titration, as described previously [43]. HCl (6 N) was purchased from Fisher Scientific (Fair Lawn, NJ), while the NaOH

was purchased from VWR (West Chester, PA). All materials were used as received.

## 2.2. Micro- and nanogel preparation

The particles were prepared from parent chitosan and TPP solutions at matching ionic strength and pH-levels, which were adjusted using NaCl, HCl and NaOH (such that the cationic chitosan had  $\text{Cl}^-$  counterions and the anionic TPP had  $\text{Na}^+$  counterions). To ensure that the free TPP concentration stayed essentially constant during the aggregation experiments, the chitosan/TPP particles were first prepared at the 0.20:1 TPP:glucosamine molar ratios (where the internal chitosan binding sites within the particles, which can adsorb TPP from solution, were nearly saturated [19]). These particles were prepared through a dropwise addition of 1 mL of 0.16 wt% (4.4 mM) TPP solution to 10 mL of 0.04 wt% (2.2 mM in its glucosamine units) chitosan solution (both at pH 4.0 and 150 mM NaCl) while stirring at 800 rpm with a 8 mm  $\times$  3 mm cylindrical stir bar. The resulting dispersions were then left to stir overnight. To quantify their aggregation kinetics at different TPP concentrations, additional 2–9 mL of 0.16 wt% TPP solution (also at pH 4.0 and 150 mM NaCl) were rapidly added to the particle dispersions to trigger their aggregation. The mixtures were then stirred for 5 s to ensure thorough mixing and transferred to dynamic light scattering (DLS) sample cells to monitor changes in their average particle size.

When the parent chitosan and TPP solutions contained NaCl, the resulting particle size depended on the NaCl concentration. This size variability made the aggregation rates at different NaCl concentrations difficult to directly compare. To avoid this problem, all particles were first prepared at the same ionic strength by adding 1 mL of 0.32 wt% TPP solution to 10 mL of 0.08 wt% chitosan (at pH 4.0 with 150 mM NaCl) and stirring the mixture overnight. Five mL of the resulting dispersion were then diluted with 5 mL of 0, 50, 100, 150 or 200 mM NaCl solution (also at pH 4.0) to achieve a final chitosan concentration of 0.036 wt% and final NaCl concentrations of 75, 100, 125, 150 or 175 mM. Ten min after dilution, the final dispersions were tested by DLS to confirm that the particle size distributions did not change. Then, 3-mL aliquots of 0.16 wt% TPP solution at corresponding NaCl concentrations were rapidly added to the particle dispersions to trigger aggregation. The samples were stirred for 5 s and immediately transferred to a DLS sample cell for the size evolution measurements.

Similarly, to test the pH-effects on the coagulation kinetics, the pH-values of preformed particle dispersions (prepared as described in the previous paragraph at pH 4.0 and 150 mM NaCl) were carefully adjusted to 3.50, 3.75, 4.00, 4.25 or 4.50 (using 0.1 M HCl and NaOH solutions) and equilibrated for 10 min. The samples were then probed by DLS to ensure the particle size distribution did not change during the pH adjustment. Then, 3 mL of 0.16 wt% TPP solution (at a matching pH) was rapidly added to each dispersion and stirred for 5 s before monitoring the dispersion for aggregation by DLS.

To investigate the DD effect on the aggregation kinetics, chitosan/TPP particles were prepared using chitosan with 72, 82, 91 and 95% DD-values. Here, the chitosans with 72, 82 and 95% DD-values (and fairly similar  $M_v$ -values of 76 kDa, 73 kDa and 57 kDa, respectively) were prepared as described previously [42], using standard deacetylation and reacetylation procedures. Particles from chitosan with 72, 82 and 91% DD-values were formed by adding 4.0, 3.6 or 3.2 mL of 0.1 wt% (2.8 mM) TPP to 10 mL of 0.1 wt% chitosan solution (both at pH 4.0) while stirring at 800 rpm, so that each final mixture was at a 0.2:1 TPP:glucosamine molar ratio. Each dispersion was then stirred overnight, whereupon 4 mL of each sample were diluted by 6 mL of 41.7 mM NaCl solution (pH 4.0) to achieve a final NaCl concentration of 25 mM.

Conversely, to ensure similar particle size and low polydispersity, particles prepared from 95% DD chitosan were formed by adding 4.2 mL of 0.04 wt% (1.1 mM) TPP to 10 mL of 0.04 wt% chitosan solution (both at pH 4.0 and 25 mM NaCl) while stirring at 800 rpm. The resulting dispersion was stirred overnight, whereupon 10 mL of the mixture (which were to be used for the aggregation kinetics measurements) were moved into a new 20 mL scintillation vial. The final particles obtained using the four different DD-values all had similar z-average diameters (of roughly 130 nm, as determined by DLS) and were all at the 0.2:1 TPP:glucosamine ratio. To trigger their aggregation, either 0.15 or 1.5 mL of 0.16 wt% (4.4 mM) TPP solution (at pH 4.0 and 25 mM NaCl) were added to the 10 mL chitosan/TPP dispersion samples. Each sample was stirred for 5 s and immediately transferred to a DLS sample cell to monitor its size evolution.

## 2.3. Light scattering analyses

Analyses of chitosan/TPP micro- and nanogel size and aggregation kinetics were primarily performed via DLS, using a Zetasizer Nano ZS dynamic and electrophoretic instrument (Malvern, UK), at  $\lambda = 633$  nm and a scattering angle of  $173^\circ$ . The initial particle sizes and polydispersity indices (PDI) were determined via the cumulant analysis as described previously [19]. Conversely, chitosan/TPP particle aggregation kinetics were quantified by tracking the temporal hydrodynamic size change at the onset of their aggregation. Once excess TPP was added to trigger particle aggregation (see Section 3.2), their z-average hydrodynamic radii (obtained through the cumulant analysis of DLS data) were tracked until they increased by 25%. As shown in Fig. 1, the increase in their normalized radii,  $r_t/r_0$  (where  $r_t$  is the radius at time  $t$  and  $r_0$  is the initial radius) in these initial aggregation stages was linear. The slopes obtained from the  $r_t/r_0$  versus  $t$  plots were then used to obtain the aggregation rate constant  $k_{11}$ , defined based on Fuchs' expression [44]:

$$\frac{dN_1}{dt} = -k_{11}N_1^2 \quad (1)$$

where  $N_1$  was the concentration of unaggregated (singlet) particles. This  $k_{11}$  was found by assuming that: (1) the only aggregation occurring at short times is that of singlets into doublets; and (2) that the scattering from the particles obeys the Rayleigh-Gans-Debye (RGD) scattering theory [37]. This assumption was made based on the criterion that  $4\pi r|m - 1|/\lambda \ll 1$  (where  $m$  is the refractive index ratio between the particle and the medium) [37] – i.e., based on the refractive index of chitosan/TPP particles that was estimated from their chitosan content (around 1.37, via the analysis in Section 3.5),  $4\pi r|m - 1|/\lambda \sim 0.01$ – $0.1$ . Accordingly,  $k_{11}$  was obtained by solving the following equation [37,45]:

$$\frac{1}{r_0} \left( \frac{dr_t}{dt} \right)_{t \rightarrow 0} = \left( \frac{\sin(2r_0 q)}{2r_0 q} + 1 \right) k_{11} N_0 \left( 1 - \frac{r_0}{r_{h,2}} \right) \quad (2)$$

where  $\frac{1}{r_0} \left( \frac{dr_t}{dt} \right)_{t \rightarrow 0}$  is the normalized rate of hydrodynamic radius change (which equals to the slope of the normalized size evolution curve),  $N_0$  is the initial particle concentration,  $r_0/r_{h,2}$  is the ratio of hydrodynamic radii between the singlets and doublets (which equals 0.725, assuming that the particles do not coalesce) [37], and  $q$  is the light scattering vector. Moreover,  $q$  is calculated as:

$$q = \left( \frac{4\pi n_0}{\lambda} \right) \sin \left( \frac{\theta}{2} \right) \quad (3)$$

where  $\lambda$  is the wavelength of the light source,  $n_0$  is the refractive index of the suspending medium,  $\theta$  is the angle between the incident light and the detector.

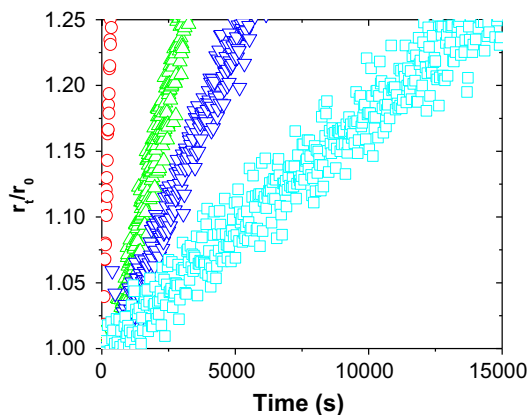


**Fig. 1.** Representative DLS data showing the normalized size evolutions of chitosan/TPP particles (prepared from 91% DD chitosan at a 0.2:1 TPP:glucosamine molar ratio) and (○) 100 mM, (△) 125 mM, (▽) 150 mM and (□) 175 mM NaCl. These data sets were collected at pH 4.0 and in the presence of 1.0 mM excess TPP ( $n = 3$ ).

To confirm the validity of the  $k_{11}$ -values obtained using the RGD theory-based DLS analysis,  $k_{11}$ -values were also calculated using a combined DLS + static light scattering (SLS) analysis, which relaxes the RGD scattering assumption. These calculations were made based on changes in both the particle radius and average (static) light scattering intensity,  $I(q,t)$  as [37,45]:

$$\frac{1}{r_0} \left( \frac{dr_t}{dt} \right)_{t=0} = \left[ \frac{1}{I(q,0)} \left( \frac{dI(q,t)}{dt} \right)_{t=0} + k_{11}N_0 \right] \left( 1 - \frac{r_0}{r_{h,2}} \right) \quad (4)$$

where  $I(q,0)$  is the initial light scattering intensity from the dispersion and  $I(q,t)$  is the light scattering intensity at time  $t$ . This DLS + SLS analysis yielded very similar  $k_{11}$ -values to those obtained using the RGD theory-based DLS analysis (Supplementary Data, Fig. S1) and validated the DLS-based  $k_{11}$ -estimates. Consequently, and because data collected by the DLS + SLS method was less precise (i.e.,  $dI(q,t)/dt$  at the  $173^\circ$  scattering angle was so small that its goodness of fit was limited by the scatter in the  $I(q,t)$  data), the remainder of this paper focuses solely on the DLS-based  $k_{11}$ -values. Each light scattering measurement was reproduced three times to obtain average values and standard deviations.

#### 2.4. Electrophoretic light scattering

The apparent  $\zeta$ -potentials of the micro- and nanogels were obtained via electrophoretic light scattering. This was achieved using the Zetasizer Nano ZS instrument (Malvern, UK), where the  $\zeta$ -potentials were estimated from the electrophoretic mobility using the Smoluchowski model [46]. These measurements were performed on all chitosan/TPP dispersions used in the aggregation rate tests, which were analyzed immediately after excess TPP addition. Each  $\zeta$ -potential measurement was repeated thrice.

#### 2.5. Capillary viscometry

To determine  $N_0$ , the relative viscosity,  $\eta_r$ , was determined using a Cannon-Ubbelohde dilution capillary viscometer (Size 75; Cannon Instrument Co., State College, PA). This was achieved by dividing the particle dispersion viscosity,  $\eta$ , by the solvent viscosity,  $\eta_s$ , from which the particle volume fraction,  $\phi$ , was estimated by Einstein's theory, which assumes the particles to be rigid spheres [28]:

$$\eta_r = \frac{\eta}{\eta_s} = 1 + 2.5\phi + k_1\phi^2 + \dots \quad (5)$$

Because the volume fraction of chitosan/TPP microgels was only 1–2%, the higher-order terms in Eq. (5) (e.g.,  $k_1\phi^2$ ) were negligible. The  $N_0$  was therefore calculated by dividing  $\phi$  by the volume of a single particle:

$$N_0 = \frac{\phi}{\frac{4}{3}\pi r_0^3} \quad (6)$$

This estimation was reasonable because the particle PDI-values were low (below 0.13 for all tests used for the  $N_0$  quantification), which ensured reliable  $r_0$ -values for the number concentration calculation. To ensure reproducibility, each viscosity measurement was repeated thrice.

### 3. Results and discussion

#### 3.1. Ionic strength effect

The first effect examined was that of ionic strength (i.e., the NaCl concentration effect). Similar to the particle formation rates reported by us earlier [26], chitosan/TPP particle aggregation rates diminished sharply with the NaCl concentration (see Fig. 1). When the NaCl concentration was 100 mM, the normalized hydrodynamic particle radius ( $r_0/r_t$ ) increased to 1.25 within 10 min. When the NaCl concentration was gradually increased to 175 mM, however, the time required for the same size increase was extended to roughly 4 h. This enhanced colloidal stability at higher monovalent salt concentrations further confirmed our previous findings, where higher excess TPP concentrations were required to aggregate chitosan/TPP microgels in the presence of 150 mM NaCl than in the absence of added NaCl [19].

After fitting these curves to Eq. (2) (in Section 2.3), the  $k_{11}N_0$ -values at each NaCl concentration were obtained (Table 1). The  $N_0$ -value was then determined via capillary viscometry to calculate  $k_{11}$ . Notably, the micro- and nanogel volume fraction determined by this analysis also enabled the determination of the chitosan content within the particles (i.e., by dividing the overall chitosan concentration by  $\phi$  [47]). Thus, based on a 0.073 wt% overall chitosan concentration and a  $\phi$  of 1.03 vol% (measured in 150 mM NaCl at pH 4.0), the particles were estimated to contain roughly 7.1 wt% chitosan. This very low polymer content was consistent with those reported by other groups [22,34]. Moreover, it suggested a highly swollen micro- and nanogel structure and, consequently, a very weak van der Waals attraction between the micro- and nanogels (*vide infra*). Likewise, as shown by the virtually constant  $r_0$  and  $\zeta$ -potential in Table 1, the polymer content within the particles (which were all prepared in 150 mM NaCl) was largely unaffected by the variations in the ambient NaCl concentration. This invariance in particle size and composition shows that their swelling remains unchanged and confirms that the only significant change in the chitosan/TPP dispersions was their ionic strength.

As indicated in Table 1, the aggregation rate constant  $k_{11}$  (obtained via Eq. (9)) decreased drastically from  $1.5 \times 10^{-20}$  to  $4.6 \times 10^{-23} \text{ m}^3/\text{s}$  as the NaCl concentration increased from 75 mM to 175 mM. Plotting  $k_{11}$  against NaCl concentration (Fig. 2) revealed  $k_{11}$  to scale approximately with  $[\text{NaCl}]^{-6.8}$ . This strong dependence is qualitatively similar to that of chitosan/TPP micro- and nanogel formation rates [26], which (based on the characteristic times of the increase in light scattering intensity during their formation) were estimated to scale with  $[\text{NaCl}]^{-5.0}$ .

Though NaCl-enhanced colloidal stability has previously been reported (albeit by more-qualitative measurements) by both us and others [19,35], different explanations for this phenomenon have been proposed. One interpretation was that higher NaCl concentrations frustrate the binding of TPP ions to the chitosan/TPP



**Table 1**

Experimental parameters and fitted  $k_{11}$ -values showing the NaCl effect on the chitosan/TPP micro- and nanogel aggregation rates at pH 4.0 and in the presence of 1.0 mM excess TPP (mean  $\pm$  standard deviation).

[NaCl] (mM)	$r_0$ (nm)	$\zeta$ (mV)	$d(r_i/r_0)/dt$ (1/s)	$k_{11}N_0$ (1/s)	$N_0(1/m^3)$	$k_{11}(m^3/s)$
75	$79.8 \pm 1.1$	$21.2 \pm 0.8$	$(5.7 \pm 0.9) \times 10^{-3}$	$(2.6 \pm 0.4) \times 10^{-2}$	$(1.8 \pm 0.1) \times 10^{18}$	$(1.5 \pm 0.2) \times 10^{-20}$
100	$73.0 \pm 1.6$	$21.4 \pm 2.9$	$(8.2 \pm 1.6) \times 10^{-4}$	$(3.6 \pm 0.7) \times 10^{-3}$	$(1.8 \pm 0.1) \times 10^{18}$	$(2.0 \pm 0.4) \times 10^{-21}$
125	$81.3 \pm 1.1$	$21.6 \pm 1.1$	$(9.7 \pm 1.4) \times 10^{-5}$	$(4.5 \pm 0.6) \times 10^{-4}$	$(1.8 \pm 0.1) \times 10^{18}$	$(2.5 \pm 0.4) \times 10^{-22}$
150	$79.5 \pm 0.9$	$22.0 \pm 0.9$	$(5.2 \pm 0.5) \times 10^{-5}$	$(2.4 \pm 0.2) \times 10^{-4}$	$(1.8 \pm 0.1) \times 10^{18}$	$(1.3 \pm 0.1) \times 10^{-22}$
175	$82.1 \pm 0.5$	$22.3 \pm 0.7$	$(1.8 \pm 0.3) \times 10^{-5}$	$(8.2 \pm 1.2) \times 10^{-5}$	$(1.8 \pm 0.1) \times 10^{18}$	$(4.6 \pm 0.7) \times 10^{-23}$

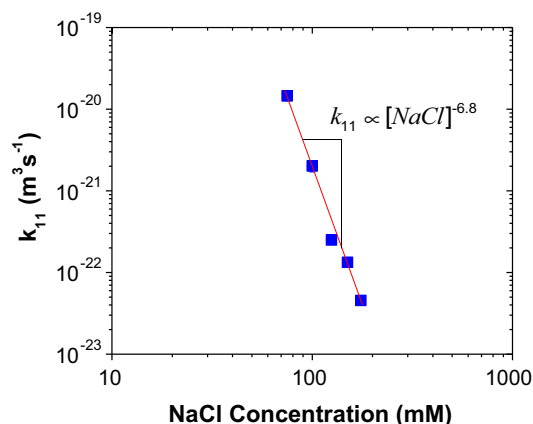


**Fig. 2.** NaCl effect on the  $k_{11}$ -values obtained at pH 4.0 and in the presence of 1.0 mM excess TPP for particles prepared from 91% DD chitosan (the solid line shows the power law fit and the error bars are standard deviations;  $n = 3$ ). Because the error bars are obscured by the symbols, the standard deviations are also provided in Table 1.

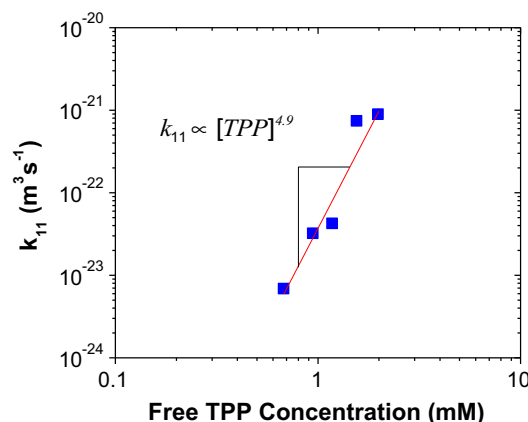


**Fig. 3.** Free TPP concentration effect on the  $k_{11}$ -values obtained at pH 4.0 and in the presence of 150 mM NaCl for particles prepared from 91% DD chitosan (the solid line is the power law fit and the error bars are standard deviations;  $n = 3$ ). Because the error bars are obscured by the symbols, the standard deviations are also provided in Table S1.

particle surfaces and inhibit their bridging flocculation (which was argued to be the primary mechanism by which these lyophilic particles aggregate) [19,27]. Another interpretation, however, attributed the high colloidal stability at elevated ionic strengths to the smaller size and higher compactness of chitosan/TPP micro- and nanogels, which was speculated to cause fewer collisions and slower chain entanglement between the colliding particles [35]. Specifically, this second interpretation argued that the smaller particle size (which prevented sedimentation-induced collisions) and slower chain entanglement counterbalanced the lower electrostatic repulsive potentials at elevated ionic strengths and led to slower aggregation [35]. This view, however, is opposed by the data in Table 1, which shows that the aggregation kinetics vary significantly even when the size, compactness and  $\zeta$ -potential remain virtually unchanged. Based on this, and the well-characterized weakening of chitosan/TPP binding in the presence of NaCl [19,42], we confirm that the enhanced colloidal stability reflects a reduction in TPP bridging.

### 3.2. TPP concentration effect

Similar measurements were also performed to investigate the effect of TPP concentration on the aggregation kinetics. Here, the pH and NaCl concentration were fixed at 4.0 and 150 mM, respectively, while varying the excess (i.e., free) TPP concentration from 0.68 to 1.98 mM. As shown in Fig. 3,  $k_{11}$  increased drastically with the TPP concentration and scaled approximately with  $[TPP]^{4.9}$ , which was identical to the scaling of the chitosan/TPP particle formation kinetics reported earlier [26]. The particle sizes and  $\zeta$ -potentials were also essentially independent of the TPP concentration (see Supplementary Data, Table S1) which, again, eliminated any possible differences in particle compactness and sedimentation properties [35]. Likewise, because the variations in

the free TPP concentrations used in this experiment had minimal impact on the Debye screening length,  $\kappa^{-1} \approx 1$  nm (i.e., the concentration of free TPP was very low relative to that of NaCl) [28], the electrostatic repulsion between the particles was hypothesized to remain virtually the same. Based on this view, the strong impact of TPP concentration on the aggregation kinetics again indicated chitosan/TPP micro- and nanogel aggregation to mainly reflect differences in TPP bridging (which can be strongly affected by the competitive binding of TPP and  $Cl^-$  ions to the particle surface). The similar NaCl and TPP concentration effects on the micro- and nanogel formation and aggregation processes might stem from their similar mechanisms; micro- and nanogel formation occurs through aggregation of primary nanoparticles [26], while the agglomeration studied here is the higher-order aggregation of larger, secondary aggregates. Moreover, the similar scaling of these rates with the free TPP concentration suggests that the aggregation of primary particles, similar to the higher-order aggregation explored here, requires their bridging by TPP.

### 3.3. pH effect

To investigate the pH effect on chitosan/TPP micro- and nanogel aggregation, preformed particles were aggregated at varying pH-values and at NaCl and excess TPP concentrations fixed at 150 mM and 0.94 mM, respectively. As indicated in Fig. 4a,  $k_{11}$  diminished from  $9.3 \times 10^{-22}$  to  $3.1 \times 10^{-24}$  m<sup>3</sup>/s as the  $H^+$  concentration increased from  $3.2 \times 10^{-5}$  to  $3.2 \times 10^{-4}$  M (i.e., as the pH was reduced from 4.5 to 3.5), where  $k_{11}$  did not follow a simple power law scaling with  $[H^+]$ . Since the effective  $pK_a$  of chitosan is around 6.0–6.5 [48,49], the protonation of the chitosan amine groups should be nearly-full and remain virtually-unchanged between pH 3.5 and 4.5. Conversely, TPP (which is a polyprotic acid with  $pK_{a,3} = 2.3$  and  $pK_{a,4} = 6.3$  [50]) changes ionization states

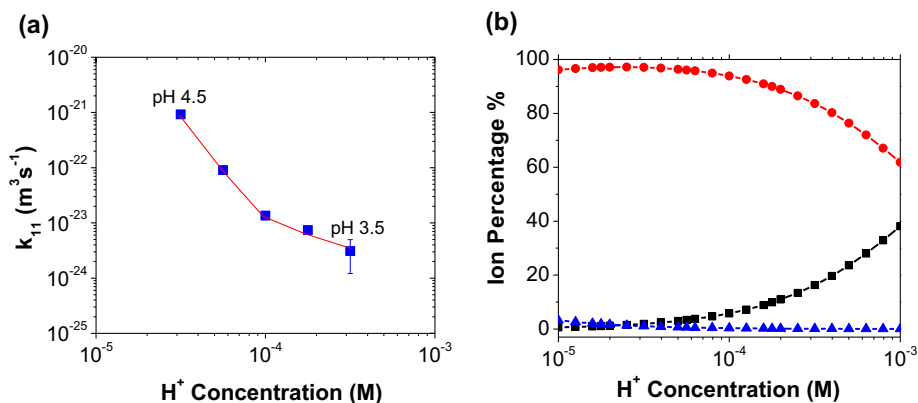


**Fig. 4.** The effect of  $H^+$  concentration on: (a) the  $k_{11}$ -values (the solid line is guide to the eyes) obtained in the presence of 150 mM NaCl and 1.0 mM free TPP (DD = 91%); and (b) the percentage of (—■—)  $TPP^{2-}$ , (—●—)  $TPP^{3-}$ , and (—▲—)  $TPP^{4-}$  in total TPP estimated from the  $pK_a$  values of TPP using the Henderson-Hasselbalch equation. The error bars are standard deviations, which are also provided in Table S2 ( $n = 3$ ).

within this pH-range. Thus, the change in aggregation kinetics likely reflects the protonation (and charge reduction) on the TPP at lower pH-values, which results in its weaker binding and diminished bridging capability.

Unlike directly changing the TPP concentration, the change in pH leads to nonlinear changes in the concentrations of free  $TPP^{2-}$ ,  $TPP^{3-}$  and  $TPP^{4-}$  ions. This nonlinear change is illustrated in Fig. 4b, which shows how the percentages TPP ions in each ionization state varied within the range of investigated pH-values (as predicted by the Henderson-Hasselbalch equation). Thus, the more-complicated trend in aggregation kinetics shown in Fig. 4a might reflect these non-linear changes in ionization. Moreover, the break in the  $k_{11}$  versus  $H^+$  concentration curve might reflect a switch in the dominant ion type underlying the changes in the aggregation rate – e.g., changing  $TPP^{3-}$  concentrations determining  $k_{11}$  at low pH-values (where there is almost no  $TPP^{4-}$ ) and changing  $TPP^{4-}$  concentrations determining  $k_{11}$  at higher pH-values (where the  $TPP^{3-}$  concentration remains virtually unchanged). Because the binding of TPP to polycations can affect its  $pK_a$ -values [51], however, no further quantitative analysis of these effects was performed.

### 3.4. DD effect

To investigate the effect of chitosan DD on the aggregation kinetics, the same experiments were repeated at different DD-values (with the pH and NaCl concentration held constant at 4.0 and 25 mM, respectively). Fig. 5 shows the  $r_t/r_0$  evolution over time when the excess TPP was added to trigger the aggregation. For particles prepared from 72% DD chitosan, the aggregation was hardly

detected when 0.57 mM excess TPP was added (Fig. 5a). The  $r_t/r_0$  increased slightly from 1.00 to 1.05 upon the addition of 0.57 mM of excess TPP and thereafter remained constant over several hours, thus indicating a very slow aggregation process and a colloidal stable dispersion. When the DD was increased to 82%, however, the aggregation rate increased drastically and the  $r_t/r_0$  rose from 1.00 to roughly 1.30 within 3 min (with macroscopic precipitation occurring within 10 min).

When the DD was further increased to 91%, the aggregation was far too rapid to be detected using 0.57 mM excess TPP. Thus, the measurements were performed using a much lower excess TPP concentration (0.065 mM). The aggregation of particles with 91% DD was slow but detectable, with  $r_t/r_0$  increasing from 1.00 to 1.15 over roughly 1 h (see Fig. 5b). The size evolution, however, became rapid again as the DD was raised by just 4% to 95%, where  $r_t/r_0$  jumped to roughly 1.15 even before the first data point was collected (i.e., within approximately 15 s) and reached 1.25 within 10 min. The burst increase in size during mixing could be explained by non-instantaneous mixing and local aggregation during TPP addition, where (before the TPP solution was fully stirred into the chitosan/TPP dispersion) the local free TPP concentration was initially much higher than 0.065 mM and resulted in more-rapid aggregation. Alternatively, at the low excess TPP concentration used in this experiment, the consumption of TPP ions by the few free chitosan amine groups might have reduced the free TPP concentration over time and therefore reduced the aggregation rate. Regardless of the reason for the burst increase, Fig. 5 showed that the aggregation kinetics of chitosan/TPP particles increased drastically with the chitosan DD-values, and likely reflected the stronger chitosan/TPP binding (which was recently demonstrated

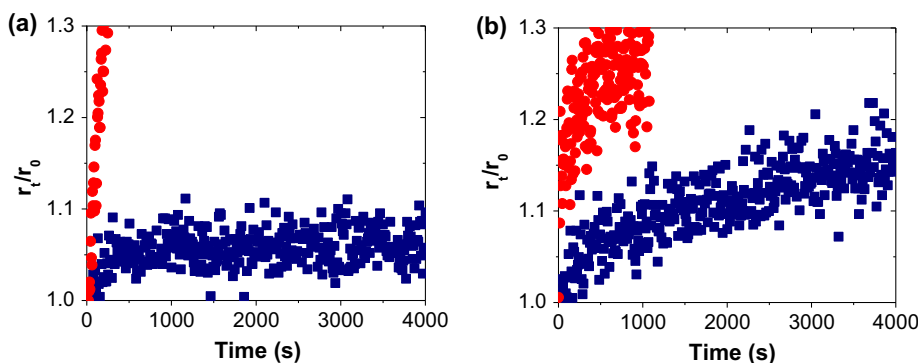


**Fig. 5.** Representative  $r_t/r_0$  evolutions in the presence of: (a) 0.57 mM excess TPP obtained using (■) 72% and (●) 82% DD chitosan; and (b) 0.065 mM excess TPP obtained using (■) 91% and (●) 95% DD chitosan (each obtained at pH 4.0 and 25 mM NaCl;  $n = 3$ ).

by isothermal titration calorimetry [42]). Thus, in addition to varying with the ionic strength, TPP concentration and pH, the aggregation kinetics can vary with the type of chitosan used, and can be sensitive to even small differences in the DD-values. This is consistent with the recent qualitative findings that the TPP:glucosamine molar ratios where the onset of rapid micro- and nanogel aggregation occurs increases substantially when the DD-value is diminished [42].

### 3.5. Comparison with theoretical predictions

As a first attempt to model chitosan/TPP micro- and nanogel aggregation, it might be useful to compare the experimental aggregation rates with theoretical predictions based on DLVO potentials, which estimate the interparticle potentials as the sum of van der Waals ( $\phi_A$ ) and electrostatic ( $\phi_E$ ) contributions [28,40,41]. These potentials are derived based on the assumption of uniformly-charged particles with smooth, well-defined boundaries. For spherical particles with uniform sizes,  $\phi_A$  and  $\phi_E$  are given by [28]:

$$\phi_A = -\frac{A}{6} \left[ \frac{2}{s^2 + 4s} + \frac{2}{s^2 + 4s + 4} + \ln \left( \frac{s^2 + 4s}{s^2 + 4s + 4} \right) \right] \quad (7)$$

$$\phi_E = 64\pi r_0 k_B T n_\infty \kappa^{-2} \Upsilon_0 \exp(-\kappa r_0 s) \quad (8a)$$

$$\Upsilon_0 = \frac{\exp(e\psi_0/2k_B T) - 1}{\exp(e\psi_0/2k_B T) + 1} \quad (8b)$$

where  $A$  is the Hamaker constant,  $s$  is the normalized surface-to-surface distance between the particles (given by the distance,  $d$ , divided by the particle radius,  $r_0$ ),  $k_B$  is the Boltzmann constant,  $T$  is the absolute temperature,  $n_\infty$  is the aqueous salt concentration,  $\kappa$  is the Debye-Hückel parameter, and  $\psi_0$  is the surface electrostatic potential of the particles, which (due to a lack of structural information about the softness of the particle surface [52,53]) was roughly estimated as the apparent  $\zeta$ -potential. Here [28]:

$$\kappa = \left( \frac{2e^2 N_A I}{\epsilon_0 \epsilon_r k_B T} \right)^{0.5} \quad (9)$$

where  $e$  is the charge of an electron,  $N_A$  is the Avogadro number,  $I$  is the ionic strength in the suspending medium,  $\epsilon_r$  is the relative dielectric constant of water and  $\epsilon_0$  is the dielectric constant of vacuum.

Based on the above potentials, the theoretical collision rate constant between identical particles can be estimated via the modified Fuchs expression as [36,54]:

$$k_{11} = \frac{4k_B T}{3\eta_s} \left[ \int_0^\infty \beta \frac{\exp[(\phi_E + \phi_A)/k_B T]}{(2+s)^2} ds \right]^{-1} \quad (10a)$$

$$\beta \approx \frac{6s^2 + 13s + 2}{6s^2 + 4s} \quad (10b)$$

which models how the frequency of collisions between smooth, spherical particles is affected by their interaction potentials (e.g., the DLVO potentials) and repulsive hydrodynamic forces, accounted for by  $\beta$  [55]. In the case of lyophobic colloids, where surface-to-surface contact between the particles always leads to aggregation, this expression is typically used to quantify the aggregation rates. In the case of the lyophilic chitosan/TPP particles, however (where not all collisions lead to aggregation), this expression only provides a collision rate constant, which will typically be faster than the aggregation rate.

As discussed in Section 3.1, the polymer content in the chitosan/TPP micro- and nanogels used in the NaCl effect experiments is

around 7.1 wt%. Accordingly, the Hamaker constant for the particles in water can be estimated from the refractive indices and dielectric constants of chitosan and water. Ignoring the effect of TPP (which constitutes less than 2% of the total particle weight), this can be done using an approximation to the Lifshitz theory proposed by Israelachvili [56,57]:

$$A_{121} \approx \frac{3}{4} k_B T \left( \frac{\epsilon_1 - \epsilon_2}{\epsilon_1 + \epsilon_2} \right)^2 + \frac{3h\nu}{16\sqrt{2}} \frac{(n_1^2 - n_2^2)^2}{(n_1^2 + n_2^2)^{3/2}} \quad (14)$$

where  $\epsilon_1$  and  $\epsilon_2$  are the respective dielectric constants for chitosan/TPP particles and water,  $h$  is Planck's constant,  $n_1$  and  $n_2$  are the refractive indices of chitosan/TPP particles and water, and  $\nu$  is the frequency of light used to measure the refractive indices [57]. The dielectric constant  $\epsilon_1$  and refractive index  $n_1$  of chitosan/TPP micro- and nanogels were estimated using the simple additive relations [57]:

$$\epsilon_1 = \phi_{cs} \epsilon_{cs} + (1 - \phi_{cs}) \epsilon_{water} \quad (15a)$$

$$n_1 = \phi_{cs} n_{cs} + (1 - \phi_{cs}) n_{water} \quad (15b)$$

where  $\epsilon_{cs}$  and  $\epsilon_{water}$  are the dielectric constants of pure chitosan (7) and water (78),  $n_{cs}$  and  $n_{water}$  are the refractive indices of pure chitosan (1.6) and water (1.33) [57], and  $\phi_{cs}$  is the volume fraction of chitosan in the particle (roughly approximated as its mass fraction – i.e., 7.1%). Combining Eqs. (14) and (15) yielded a Hamaker constant on the order of  $10^{-22}$  J, which (as expected) was very small compared to the typical values of  $10^{-20}$ – $10^{-19}$  J reported for lyophobic colloids [28]. Using this Hamaker constant, and the experimentally measured particle sizes and  $\zeta$ -potentials from Table 1, the interparticle interaction potentials were calculated using Eqs. (7) and (8) as  $\phi_A + \phi_E$  (see Fig. 6a). The electrostatic repulsive potential,  $\phi_E$  (solid line in Fig. 6a), was much higher than the van der Waals attractive potential,  $\phi_A$  (dashed line in Fig. 6a). This led to a large repulsive barrier (of roughly  $35k_B T$ ) in the net interaction potential (dotted line in Fig. 6a) and prevented the particles from colliding.

This strong repulsive energy barrier gave rise to very slow theoretical collision rates at all examined ionic strengths (solid squares in Fig. 6b). These collision rate constants (calculated using Eq. (10)) were around  $10^{-32}$ – $10^{-31}$  m<sup>3</sup>/s, and increased slightly with ionic strength due to the reduced electrostatic repulsion between the particles. These theoretical collision rates, however, were much lower than the experimental aggregation rates in Table 1 (circles in Fig. 6b), which ranged between  $10^{-20}$  and  $10^{-23}$  m<sup>3</sup>/s. Because aggregation events were expected to be less frequent than collisions for chitosan/TPP particles, this discrepancy revealed a gross theoretical underprediction of the collision and aggregation rates. Considering the uncertainty in the estimated  $A_{121}$ -value, a sensitivity analysis was also performed by increasing  $A_{121}$  by one order of magnitude (to  $10^{-21}$  J; see Supplementary Data, Fig. S2a for the interaction potentials) – i.e., to probe whether the low theoretical collision rates might reflect an underprediction of  $A_{121}$ . Even with this enhanced van der Waals attraction, however, the theoretical  $k_{11}$ -values (open triangles in Fig. 6b) were still much lower than the experimental values. Hence, the discrepancies between the experimental and theoretical  $k_{11}$ -values were likely not caused by a low  $A_{121}$  estimate.

Four other possible explanations emerge for this large deviation between the experimental and theoretical collision rates. The first is that the particles are not perfectly spherical. Because chitosan/TPP micro- and nanogels are aggregates of roughly 30-nm primary nanoparticles [26], they tend to have “raspberry-like” (or sometimes even fractal) rather than truly spherical shapes [18,26]. Indeed, TEM imaging of particles prepared at the pH and ionic strength used herein revealed a raspberry-like morphology, with

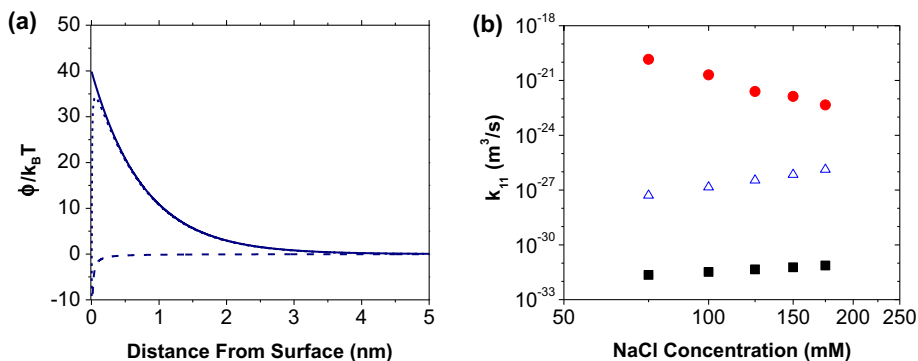


**Fig. 6.** Plots showing: (a) representative particle interaction potentials: (solid line)  $\phi_E$ , (dashed line)  $\phi_A$  and (dotted line) net potential ( $\phi_A + \phi_E$ ) versus distance from particle surface when  $A_{121} = 1 \times 10^{-22}$  J,  $\zeta = 22$  mV,  $r_0 = 80$  nm and  $[\text{NaCl}] = 150$  mM; and (b) the aggregation rate constants (●) determined experimentally via DLS (from Table 1) compared to the collision rate constants calculated using Eq. (10) when (■)  $A_{121} = 1 \times 10^{-22}$  J and (△)  $A_{121} = 1 \times 10^{-21}$  J.

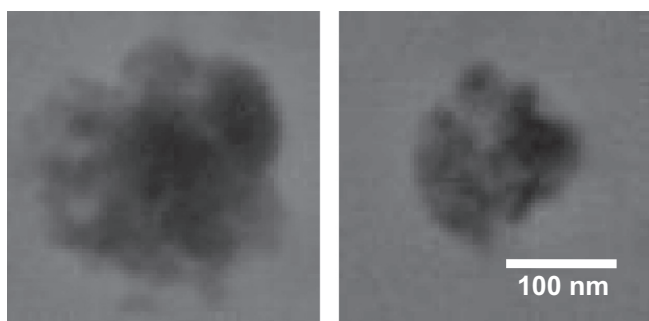


**Fig. 7.** TEM images of representative chitosan/TPP microgels prepared in 150 mM NaCl (parent chitosan and TPP solution pH = 4.0) from 90% DD chitosan. TPP: glucosamine ratio = 0.06:1. Reproduced from Ref. [26] with permission from the American Chemical Society.

clearly visible nanoscale subunits [26] (see Fig. 7). Thus, the radii of curvature governing the electrostatic repulsion between the particles may be closer to the roughly 15-nm radii of the primary particles [26] than to the 80-nm radii of the secondary particles (see Table 1 and Fig. 8a). This view is supported by the nanometer-scale range of the repulsive potential shown in Fig. 6a, which reflects the short Debye screening length and makes it likely for only the subunits that are closest to the neighboring particle to contribute to the  $\phi_E$ . Repeating the calculations in Fig. 6 using this new radius of curvature yields much lower repulsive potentials (all below  $7k_B T$ ; see Supplementary Data, Fig. S2b–f) and theoretical collision rate constants that now exceed the experimental  $k_{11}$ -values (Supplementary Data, Fig. S3). When the NaCl concentration increases from 75 to 175 mM, these new theoretical collision rates increase from  $7.2 \times 10^{-20}$  to  $9.6 \times 10^{-20}$  m<sup>3</sup>/s when  $A_{121}$  is estimated as  $10^{-22}$  J, and from  $4.5 \times 10^{-19}$  to  $8.4 \times 10^{-19}$  m<sup>3</sup>/s when  $A_{121}$  is increased tenfold to  $10^{-21}$  J. All of these values exceed the  $4.6 \times 10^{-23}$ – $1.5 \times 10^{-20}$  m<sup>3</sup>/s experimental  $k_{11}$ -values (see Table 1 and Fig. 6b) and, because aggregation events are expected to be less frequent than collisions, suggest that the raspberry-like particle shape might indeed (at least partly) account for the higher experimental aggregation rates.

As a second explanation, we postulate that the faster experimental aggregation rates also may have reflected the bridging of the polymer segments extending from the particle surfaces (Fig. 8b). Instead of having a rigid and well-defined outer boundary that is modeled by the DLVO and Fuchs theories, polymeric microgels (albeit covalently crosslinked ones) have been reported to have dangling polymer chains that can extend out far beyond the polymer-rich core [58], and the same might exist for gel-like chitosan/TPP particles. The bare persistence length of chitosan is

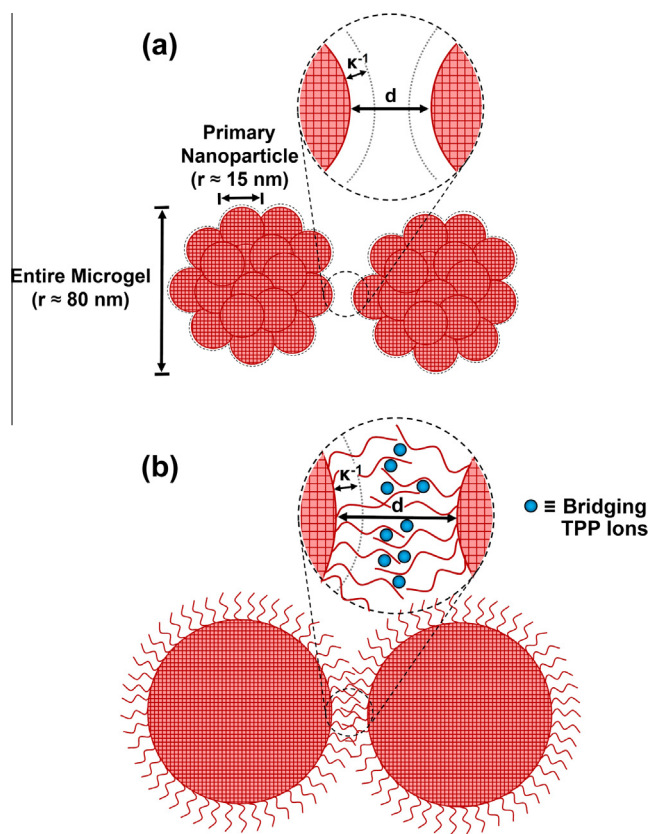


**Fig. 8.** The schematic diagrams of: (a) raspberry-like chitosan/TPP micro- and nanogel morphologies; and (b) chitosan chains extending from the particle surfaces beyond the Debye length ( $\kappa^{-1}$ ) and being bridged by TPP ions.

estimated at 6 nm [59,60], which is much greater than the roughly 1-nm Debye length in the aggregation experiments. Thus, the extended chitosan segments may easily extend beyond the double layer, especially at the 75–175 mM NaCl concentrations (where the double layer is highly compressed). These extended polyelectrolyte segments might therefore be bridged by TPP without the particles having to fully overcome the repulsive energy barrier (i.e., without requiring surface-to-surface contact; see Fig. 8b). Consequently, aggregation events might occur more frequently than the surface-to-surface collisions predicted by the Fuchs theory.

A related, third explanation is that this “soft” particle-solvent boundary may also have caused the  $\psi_0$ -values (which were used to estimate  $\phi_E$ ) to be substantially lower than the measured



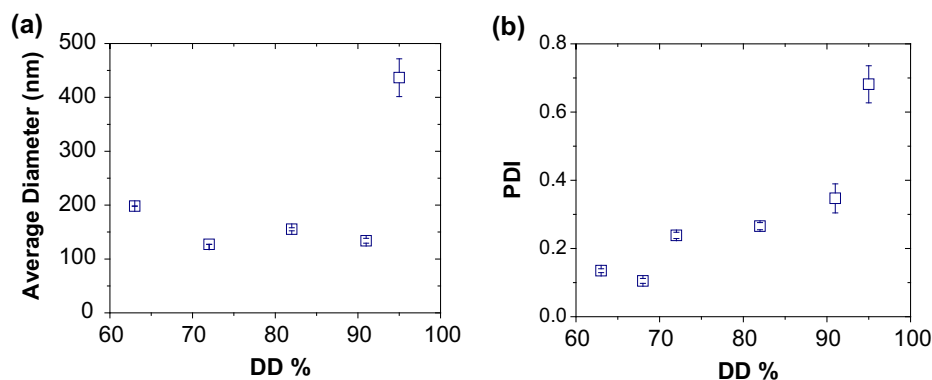


**Fig. 9.** DLS data showing estimates of the: (a) z-average hydrodynamic diameters and (b) PDI-values of chitosan/TPP particles prepared from variably deacetylated chitosans at pH 4.0 (with no added NaCl) by adding 4 mL of 0.1 wt% TPP solution into 10 mL of 0.1 wt% chitosan. The error bars are standard deviations ( $n = 3$ ).

$\zeta$ -potentials. This effect may further limit the reliability of the DLVO-based  $k_{11}$ -predictions. Though this  $\phi_E$  estimate could have potentially been improved using the Ohshima model [52,53], reliable fitting of electrophoretic mobility data to this model required: (1) knowledge of the charged outer (brush) layer thickness; and (2) electrophoretic mobility measurements at much lower (ca. 1–10 mM) NaCl concentrations. Since structural information about the outer layer thickness was unavailable (and the impact of the 10 to 100-fold reduction in NaCl concentration on this structure was uncertain), this approach was not pursued in this initial aggregation kinetics study.

The fourth and final proposed explanation for why model  $k_{11}$ -values in Fig. 6b underpredict the aggregation rates is that collisions are more rapid due to charge heterogeneity on the chitosan/TPP particle surface. Surface charge heterogeneity (which is not accounted for by the DLVO theory) can generate additional attraction between particles and has been proposed as the reason for accelerated aggregation of polystyrene latex particles in the presence of tri- and tetravalent counterions (where aggregation rates were also faster than those predicted based on DLVO potentials) [61,62]. Thus, it is possible that uneven TPP adsorption may lead to a heterogeneous chitosan/TPP particle charge and, just like in the case of the polystyrene latexes [61,62], may cause a reduction in electrostatic repulsion. Though there is no direct evidence of surface charge heterogeneity-mediated attraction in chitosan/TPP dispersions, this possibility cannot be excluded.

### 3.6. Effects on particle polydispersity

Despite the above challenges in predicting  $k_{11}$ , the new insights on chitosan/TPP particle aggregation kinetics gained through this study can be used to develop better particle preparation procedures that optimize their size and polydispersity. During particle formation, where (like in the aggregation experiments performed here) there is initially free TPP present, both primary and higher-order chitosan/TPP particles are subject to TPP-induced aggregation. To ensure the formation of particles with uniform size distributions, both particle formation and aggregation should proceed at the same rate throughout the sample. A challenge in achieving this, however, is that chitosan/TPP particles often form faster than the time required to mix the parent chitosan and TPP solutions (which causes significant particle formation/aggregation to occur before TPP is distributed throughout the sample).

One way to overcome this problem is to slow the particle formation/aggregation process down, so that the particle aggregation during mixing is limited. We have recently shown that this effect can be achieved by preparing the chitosan/TPP particles in the

presence of 150 mM NaCl (which drastically reduced particle polydispersity) [19]. The present findings, which show aggregation kinetics to also be slower at lower TPP concentrations, and lower pH and DD-values, suggest that similar effects may also be achieved by tuning other formulation parameters. To start exploring this, we have prepared particles at variable DD-values and matching chitosan and TPP concentrations (see Fig. 9). DLS analysis of these particles revealed their size distributions to become progressively more uniform at lower DD-values (where aggregation kinetics were slower), which supports the above hypothesis.

In making the above adjustments to the DD-values (or other formulation parameters), however, several complications can occur. The first reflects the fact that conditions for slow aggregation coincide with those where chitosan/TPP binding is the weakest. These conditions can either destabilize chitosan/TPP particles (i.e., cause them to dissolve) or simply interfere with their formation. At low DD-values, for instance (e.g., at 63% DD), the particles do not start forming until much higher TPP:glucosamine ratios than those required for their higher-DD counterparts [42]. Accordingly, since particles that are not fully-formed are more polydisperse [19,26], lowering the DD to the point where particle formation is inhibited can lead to higher (rather than lower) apparent PDIs. Similar effects can occur in the limit of high NaCl concentrations, which can inhibit chitosan/TPP binding and (especially at lower DD-values [42]) prevent the particles from forming [19]. In such situations, where the addition of salt causes particles to be less-fully formed, the polydispersity in the presence of salt might be higher than in its absence.

Another situation where NaCl addition fails to lower chitosan/TPP particle polydispersity is where very highly deacetylated ( $\geq 95\%$  DD) chitosan is used. Though adding NaCl still led to slower aggregation in the excess of TPP when 95% DD chitosan was used (Supplementary Data, Fig. S4), the addition of NaCl to these particles destabilized them under the TPP-limited conditions that are typically used in their preparation (i.e., below 0.2:1 TPP:glucosamine molar ratios, where without salt the particles remain stable). Instead of remaining stably dispersed at these TPP:glucosamine ratios (as when prepared under the salt-free condition), the particles prepared in 150 mM NaCl started noticeably aggregating upon their preparation, even when TPP was not in excess. Thus, when the chitosan DD-value was raised to 95%, NaCl addition to the parent chitosan and TPP solutions no longer reliably reduced the particle PDI, since NaCl caused the particles to aggregate into polydisperse flocs (data not shown).

Remarkably, this salt effect at high DD-values under TPP-limited conditions was opposite to that seen when TPP was in excess (see Fig. S4). This might be because the weakened chitosan/TPP binding in the presence of NaCl [19] increased the free

TPP concentration that remained unbound – i.e., it increased the chitosan/TPP dissociation constant. When TPP was added in excess (as done in the  $k_{11}$ -measurements), this likely had a negligible impact on the free TPP concentration, and thus did not affect the aggregation rates. Under TPP-limited conditions, however, there were only trace amounts of free TPP. Hence, the free TPP concentration probably increased much more appreciably due to the weakened chitosan/TPP binding in the presence of NaCl. Because aggregation rates were acutely sensitive to the free TPP concentrations (see Fig. 3), this increase in free TPP might have reduced the extent to which NaCl addition inhibited particle bridging. Accordingly, under TPP-limited conditions the salt-induced inhibition of particle bridging likely became insufficient to outweigh the increased particle collision frequency caused by the electrostatic screening and, for particles prepared from 95% DD chitosan (which, as suggested by Fig. 5b, aggregated appreciably even at low free TPP concentrations), NaCl accelerated particle aggregation and increased polydispersity.

These findings were consistent with those reported by other labs (where monovalent salt increased the PDI-values of particles prepared from 95 to 97.5% DD chitosan) [18,63], and likely reflected the stronger chitosan/TPP binding at higher DD-values [42]. When particles were formed from 91% (or lower) DD chitosan [19,35], even if the increased frequency in chitosan/TPP particle collisions at elevated ionic strengths outweighed the NaCl-mediated reduction in bridging probability, bridging events at trace free TPP concentrations were very improbable. Thus, at least on the typical timescales of particle formation and characterization, the newly-formed particles did not aggregate into polydisperse flocs in the presence of NaCl unless TPP was in excess [19,22]. Conversely, when particles were prepared from 95 to 97.5% DD chitosan, the stronger chitosan/TPP binding evidently increased the bridging probability, and (when NaCl addition increased their collision frequency) caused polydisperse particle aggregates to form over experimental timescales. This DD-value effect explains the apparent discrepancies between reports that show monovalent salt to increase the PDI-values of chitosan/TPP particles (which used 95–97.5% DD chitosan) [18,63] and reports that showed the monovalent salt to decrease the PDI and enhance the colloidal stability of chitosan/TPP particles (which used 83–90% DD chitosan) [19,35]. In other words, at very high DD-values, the trace amounts of TPP that remained available to bind to the particle surface at TPP:glucosamine ratios below 0.2:1 were sufficient to result in bridging flocculation, even when the chitosan/TPP binding was weakened by monovalent salt, and (unlike the chitosan/TPP particles with lower DD-values) caused the dispersions to be destabilized by NaCl addition. This effect, along with those of NaCl, pH and DD on particle dissolution stability [42], must be carefully considered when tailoring chitosan/TPP micro- and nanogel formation/aggregation kinetics.

#### 4. Conclusions

To quantify the aggregation events that determine chitosan/TPP micro- and nanogel size distributions [26,27], chitosan/TPP microgel aggregation rate constants were measured for the first time. The aggregation rates increase sharply with the free TPP concentration and decrease sharply with the monovalent salt concentration. Likewise, the aggregation rates increase with the pH (at least while the pH remains far below the effective chitosan  $pK_a$ ) and with the chitosan DD. These differences in aggregation rates apparently reflect the variations in the strength of TPP binding to the particle surface and, thus, its ability to bridge the particles together. Moreover, because these variations in aggregation rates were obtained using particles with the same size, they

confirm that the monovalent salt-induced stabilization of chitosan/TPP dispersions is caused by weakened TPP binding [19], and not (as alternatively proposed) changes in chitosan/TPP particle size and compactness [35].

Interestingly, the measured aggregation rates are much faster than those predicted based on DLVO interaction potentials. This might either reflect the presence of polymer segments extending from the particle surface, nonuniformities in particle shape (which is raspberry-like rather than spherical) and charge, or uncertainty in their overall surface potential estimate. These complicating factors, along with the observed disparity between experiment and theory, highlight the complexity in theoretically predicting the aggregation rate constants for ionically crosslinked micro- and nanogels.

Also analyzed were the implications of these aggregation kinetics on the uniformity of chitosan/TPP micro- and nanogel size, which: (1) revealed how particle polydispersity can be diminished by lowering the chitosan DD; and (2) suggested that the opposing results on how chitosan/TPP particle polydispersity is affected by monovalent salt [18,19] are likely a chitosan DD effect. Aside from tuning polydispersity, the improved understanding of the parameters governing chitosan/TPP particle aggregation may enable better strategies for tuning the average size of chitosan/TPP particles (and possibly of even other ionically crosslinked colloids [64]). Similarly, the aggregation rate constants obtained herein may ultimately enable predictive, theoretical (i.e., population balance [65]) modelling of chitosan/TPP micro- and nanogel formation, which could provide even better guidelines for tailoring their sizes to their various potential applications.

#### Acknowledgement

We are grateful to the National Science Foundation (CBET-1133795) for supporting this work and Dr. Michael Rubinstein (Univ. of North Carolina) for a helpful discussion.

#### Appendix A. Supplementary material

Supplementary data associated with this article can be found, in the online version, at <http://dx.doi.org/10.1016/j.jcis.2016.09.050>.

#### References

- [1] P. Calvo, C. Remunan-Lopez, J.L. Vila-Jato, M.J. Alonso, Chitosan and chitosan/ethylene oxide-propylene oxide block copolymer nanoparticles as novel carriers for proteins and vaccines, *Pharm. Res.* 14 (1997) 1431–1436.
- [2] P. Calvo, C. Remunan-Lopez, J.L. Vila-Jato, M.J. Alonso, Novel hydrophilic chitosan-polyethylene oxide nanoparticles as protein carriers, *J. Appl. Polym. Sci.* 63 (1997) 125–132.
- [3] N. Csaba, M. Koping-Hoggard, M.J. Alonso, Ionically crosslinked chitosan/tripolyphosphate nanoparticles for oligonucleotide and plasmid DNA delivery, *Int. J. Pharm.* 382 (2009) 205–214.
- [4] A.M. De Campos, A. Sanchez, M.J. Alonso, Chitosan nanoparticles: a new vehicle for the improvement of the delivery of drugs to the ocular surface, *Int. J. Pharm.* 224 (2001) 159–168.
- [5] Q. Gan, T. Wang, Chitosan nanoparticle as protein delivery carrier-systematic examination of fabrication conditions for efficient loading in release, *Colloids Surf. B* 59 (2007) 24–34.
- [6] M. Garcia-Fuentes, M.J. Alonso, Chitosan-based drug nanocarriers: where do we stand?, *J. Controlled Release* 161 (2012) 496–504.
- [7] Z. Ma, H.H. Yeoh, L.Y. Lim, Formulation pH modulates the interaction of insulin with chitosan nanoparticles, *J. Pharm. Sci.* 91 (2002) 1396–1404.
- [8] X. Wang, N. Chi, X. Tang, Preparation of estradiol chitosan nanoparticles for improving nasal absorption and brain targeting, *Eur. J. Pharm. Biopharm.* 70 (2008) 735–740.
- [9] C. Colonna, B. Conti, P. Perugini, F. Pavanetto, T. Modena, Chitosan glutamate nanoparticles for protein delivery: development and effect on prolidase stability, *J. Microencapsulation* 24 (2007) 553–564.
- [10] C.M. Lehr, J.A. Bouwstra, E.H. Schacht, H.E. Junginger, In vitro evaluation of mucoadhesive properties of chitosan and some other natural polymers, *Int. J. Pharm.* 78 (1992) 43–48.

- [11] D. Vilasaliu, R. Exposito-Harris, A. Heras, L. Casettari, M. Garnett, L. Illum, et al., Tight junction modulation by chitosan nanoparticles: comparison with chitosan solution, *Int. J. Pharm.* 400 (2010) 183–193.
- [12] A.M. de Campos, Y. Diebold, E.L.S. Carvalho, A. Sanchez, M.J. Alonso, Chitosan nanoparticles as new ocular drug delivery systems: in vitro stability, in vivo fate, and cellular toxicity, *Pharm. Res.* 21 (2004) 803–810.
- [13] R. Fernandez-Urrusuno, P. Calvo, C. Remunan-Lopez, J.L. Vila-Jato, M.J. Alonso, Enhancement of nasal absorption of insulin using chitosan nanoparticles, *Pharm. Res.* 16 (1999) 1576–1581.
- [14] B. Hu, C.L. Pan, Y. Sun, Z.Y. Hou, H. Ye, X.X. Zeng, Optimization of fabrication parameters to produce chitosan-tripolyphosphate nanoparticles for delivery of tea catechins, *J. Agric. Food Chem.* 56 (2008) 7451–7458.
- [15] H. Katas, H.O. Alpar, Development and characterisation of chitosan nanoparticles for siRNA delivery, *J. Controlled Release* 115 (2006) 216–225.
- [16] W. Fan, W. Yan, Z.S. Xu, H. Ni, Formation mechanism of monodisperse, low molecular weight chitosan nanoparticles by ionic gelation technique, *Colloids Surf. B* 90 (2012) 21–27.
- [17] Q. Gan, T. Wang, C. Cochrane, P. McCarron, Modulation of surface charge, particle size and morphological properties of chitosan-TPP nanoparticles intended for gene delivery, *Colloids Surf. B* 44 (2005) 65–73.
- [18] L. Bugnicourt, P. Alcouffe, C. Ladaviere, Elaboration of chitosan nanoparticles: favorable impact of a mild thermal treatment to obtain finely divided, spherical, and colloidal stable objects, *Colloids Surf. A* 457 (2014) 476–486.
- [19] Y. Huang, Y. Lapitsky, Monovalent salt enhances colloidal stability during the formation of chitosan/tripolyphosphate microgels, *Langmuir* 27 (2011) 10392–10399.
- [20] A. Nasti, N.M. Zaki, P. de Leonardis, S. Ungphaiboon, P. Sansongsak, M.G. Rimoli, et al., Chitosan/TPP and chitosan/TPP-hyaluronic acid nanoparticles: systematic optimisation of the preparative process and preliminary biological evaluation, *Pharm. Res.* 26 (2009) 1918–1930.
- [21] H. Zhang, M. Oh, C. Allen, E. Kumacheva, Monodisperse chitosan nanoparticles for mucosal drug delivery, *Biomacromolecules* 5 (2004) 2461–2468.
- [22] H. Jonassen, A.L. Kjoniksen, M. Hiorth, Effects of ionic strength on the size and compactness of chitosan nanoparticles, *Colloid Polym. Sci.* 290 (2012) 919–929.
- [23] A. Grenha, B. Seijo, C. Remunan-Lopez, Microencapsulated chitosan nanoparticles for lung protein delivery, *Eur. J. Pharm. Sci.* 25 (2005) 427–437.
- [24] R. Fernandez-Urrusuno, D. Romani, P. Calvo, J.L. Vila-Jato, M.J. Alonso, Development of a freeze-dried formulation of insulin-loaded chitosan nanoparticles intended for nasal administration, *STP Pharm. Sci.* 9 (1999) 429–436.
- [25] M.L. Tsai, S.W. Bai, R.H. Chen, Cavitation effects versus stretch effects resulted in different size and polydispersity of ionotropic gelation chitosan–sodium tripolyphosphate nanoparticle, *Carbohydr. Polym.* 71 (2008) 448–457.
- [26] Y. Huang, Y. Lapitsky, Salt-assisted mechanistic analysis of chitosan/tripolyphosphate micro- and nanogel formation, *Biomacromolecules* 13 (2012) 3868–3876.
- [27] Y. Lapitsky, Ionically crosslinked polyelectrolyte nanocarriers: recent advances and open problems, *Curr. Opin. Colloid Interface Sci.* 19 (2014) 122–130.
- [28] P.C. Hiemenz, R. Rajagopalan, Principles of Colloid and Surface Chemistry, Marcel Dekker, Inc., New York, 1997.
- [29] J.Z. Wu, G. Huang, Z.B. Hu, Interparticle potential and the phase behavior of temperature-sensitive microgel dispersions, *Macromolecules* 36 (2003) 440–448.
- [30] B.R. Saunders, B. Vincent, Microgel particles as model colloids: theory, properties and applications, *Adv. Colloid Interface Sci.* 80 (1999) 1–25.
- [31] J. Israelachvili, H. Wennerström, Role of hydration and water structure in biological and colloidal interactions, *Nature* 379 (1996) 219–225.
- [32] R.H. Pelton, P. Chibante, Preparation of aqueous latices with N-isopropylacrylamide, *Colloids Surf.* 20 (1986) 247–256.
- [33] J.Z. Wu, G. Huang, Z.B. Hu, Phase behavior of thermally responsive microgel colloids, *Phys. Rev. Lett.* 90 (2003) 048304.
- [34] J. Li, Q. Huang, Rheological properties of chitosan-tripolyphosphate complexes: from suspensions to microgels, *Carbohydr. Polym.* 87 (2012) 1670–1677.
- [35] H. Jonassen, A.L. Kjoniksen, M. Hiorth, Stability of chitosan nanoparticles cross-linked with tripolyphosphate, *Biomacromolecules* 13 (2012) 3747–3756.
- [36] S.H. Behrens, D.I. Christl, R. Emmerzael, P. Schurtenberger, M. Borkovec, Charging and aggregation properties of carboxyl latex particles: experiments versus DLVO theory, *Langmuir* 16 (2000) 2566–2575.
- [37] H. Holthoff, S.U. Egelhaaf, M. Borkovec, P. Schurtenberger, H. Sticher, Coagulation rate measurements of colloidal particles by simultaneous static and dynamic light scattering, *Langmuir* 12 (1996) 5541–5549.
- [38] J.H. Van Zanten, M. Elimelech, Determination of absolute coagulation rate constants by multiangle light scattering, *J. Colloid Interface Sci.* 154 (1992) 1–7.
- [39] M. Garcia-Salinas, M. Romero-Cano, Nieves F. De Las, Colloidal stability of a temperature-sensitive poly (N-isopropylacrylamide/2-acrylamido-2-methylpropanesulphonic acid) microgel, *J. Colloid Interface Sci.* 248 (2002) 54–61.
- [40] B. Deryagin, L. Landau, Theory of the stability of strongly charged lyophobic sols and of the adhesion of strongly charged particles in solutions of electrolytes, *Acta Physicochim. URSS* 14 (1941) 633–662.
- [41] E.J.W. Verwey, J.T.G. Overbeek, Theory of the stability of lyophobic colloids, *J. Colloid Sci.* 10 (1955) 224–225.
- [42] Y. Huang, Y. Cai, Y. Lapitsky, Factors affecting the stability of chitosan/tripolyphosphate micro- and nanogels: resolving the opposing findings, *J. Mater. Chem. B* 3 (2015) 5957–5970.
- [43] Y. Lapitsky, T. Zahir, M.S. Shoichet, Modular biodegradable biomaterials from surfactant and polyelectrolyte mixtures, *Biomacromolecules* 9 (2008) 166–174.
- [44] N. Fuchs, Über die stabilität und aufladung der aerosole, *Z. Physik.* 89 (1934) 736–743.
- [45] H. Holthoff, A. Schmitt, A. Fernandez-Barbero, M. Borkovec, M.A. Cabrerizo-Vilchez, P. Schurtenberger, et al., Measurement of absolute coagulation rate constants for colloidal particles: comparison of single and multiparticle light scattering techniques, *J. Colloid Interface Sci.* 192 (1997) 463–470.
- [46] Robert J. Hunter, R.H. Ottewill, R.L. Rowell, Zeta Potential in Colloid Science, Elsevier Ltd., New York, 1981.
- [47] Y. Cai, Y. Lapitsky, Formation and dissolution of chitosan/pyrophosphate nanoparticles: is the ionic crosslinking of chitosan reversible?, *Colloids Surf. B* 115 (2014) 100–108.
- [48] C.K.S. Pillai, W. Paul, C.P. Sharma, Chitosan and chitosan polymers: chemistry, solubility and fiber formation, *Prog. Polym. Sci.* 34 (2009) 641–678.
- [49] P. Sorlier, A. Denuziere, C. Viton, A. Domard, Relation between the degree of acetylation and the electrostatic properties of chitin and chitosan, *Biomacromolecules* 2 (2001) 765–772.
- [50] R. Laus, T.G. Costa, B. Szpoganicz, V.T. Favere, Adsorption and desorption of Cu (II), Cd(II) and Pb(II) ions using chitosan crosslinked with epichlorohydrin-tripolyphosphate as the adsorbent, *J. Hazard. Mater.* 183 (2010) 233–241.
- [51] P.G. Lawrence, Y. Lapitsky, Ionically crosslinked poly(allylamine) as a stimulus-responsive underwater adhesive: ionic strength and pH effects, *Langmuir* 31 (2015) 1564–1574.
- [52] H. Ohshima, Electrokinetics of soft particles, *Colloid Polym. Sci.* 285 (2007) 1411–1421.
- [53] H. Ohshima, T. Kondo, Approximate analytic expression for the electrophoretic mobility of colloidal particles with surface-charge layers, *J. Colloid Interface Sci.* 130 (1989) 281–282.
- [54] W.B. Russel, D.A. Saville, W.R. Schowalter, Colloidal Dispersions, Cambridge University Press, Cambridge, 1989.
- [55] E.P. Honig, G.J. Roeberson, P.H. Wiersma, Effect of hydrodynamic interaction on the coagulation rate of hydrophobic colloids, *J. Colloid Interface Sci.* 36 (1971) 97–109.
- [56] J. Israelachvili, Intermolecular & Surface Forces, second ed., Academic Press, London, 1992.
- [57] M. Holmberg, J. Berg, S. Stemme, L. Oedberg, J. Rasmussen, P. Claesson, Surface force studies of Langmuir-Blodgett cellulose films, *J. Colloid Interface Sci.* 186 (1997) 369–381.
- [58] T. Eckert, W. Richtering, Thermodynamic and hydrodynamic interaction in concentrated microgel suspensions: hard or soft sphere behavior?, *J. Chem. Phys.* 129 (2008) 124902/1–124902/6.
- [59] A.B. Kayitmazer, D. Shaw, P.L. Dubin, Role of polyelectrolyte persistence length in the binding of oppositely charged micelles, dendrimers, and protein to chitosan and poly(dimethyldiallylammonium chloride), *Macromolecules* 38 (2005) 5198–5204.
- [60] G. Berth, H. Colfen, H. Dautzenberg, Physicochemical and chemical characterisation of chitosan in dilute aqueous solution, in: E. Borchard, A. Straatmann (Eds.), Analytical Ultracentrifugation VI, Springer-Verlag, Berlin, 2002, pp. 50–57.
- [61] P. Sinha, I. Szilagyi, F.J.M. Ruiz-Cabello, P. Maroni, M. Borkovec, Attractive forces between charged colloidal particles induced by multivalent ions revealed by confronting aggregation and direct force measurements, *J. Phys. Chem. Lett.* 4 (2013) 648–652.
- [62] I. Szilagyi, A. Polomska, D. Citherlet, A. Sadeghpour, M. Borkovec, Charging and aggregation of negatively charged colloidal latex particles in the presence of multivalent oligoamine cations, *J. Colloid Interface Sci.* 392 (2013) 34–41.
- [63] Y. Wu, W. Yang, C. Wang, J. Hu, S. Fu, Chitosan nanoparticles as a novel delivery system for ammonium glycyrrhizinate, *Int. J. Pharm.* 295 (2005) 235–245.
- [64] S. Pistone, D. Qoragllu, G. Smistad, M. Hiorth, Formulation and preparation of stable cross-linked alginate–zinc nanoparticles in the presence of a monovalent salt, *Soft Matter* 11 (2015) 5765–5774.
- [65] A. Eitzlmayr, C. Petschacher, S. Radl, D. Suzzi, A. Zimmer, J.G. Khinast, Modeling and simulation of polyacrylic acid/protamine nanoparticle precipitation, *Soft Matter* 7 (2011) 9484–9497.